

The Dark Matter distribution function and Halo Thermalization from the Eddington equation in Galaxies

H. J. de Vega ^{(a,b)*} and N. G. Sanchez ^{(b)†}

^(a) *LPTHE, Université Pierre et Marie Curie (Paris VI),
Laboratoire Associé au CNRS UMR 7589, Tour 24, 5ème. étage,
Boite 126, 4, Place Jussieu, 75252 Paris, Cedex 05, France.*

^(b) *Observatoire de Paris, LERMA. Laboratoire Associé au CNRS UMR 8112.
61, Avenue de l'Observatoire, 75014 Paris, France.*

(Dated: December 3, 2024)

We find the distribution function $f(E)$ for dark matter (DM) halos in galaxies and the corresponding equation of state from the observed (empirical) DM halo density profiles. We solve for DM in galaxies the analogous of the Eddington equation originally used for the gas of stars in globular clusters. The observed density profiles are a good realistic starting point and the distribution functions derived from them are realistic. We do not make any assumption about the DM nature, the methods developed here apply to any DM kind, though all results are consistent with Warm DM (WDM). Cored density profiles behaving quadratically for small distances $\rho(r) \stackrel{r \rightarrow 0}{\approx} \rho(0) - K r^2$ produce distribution functions which are finite and positive at the halo center while cusped density profiles always produce divergent distribution functions at the center. Cored density profiles produce thermal Boltzmann distribution functions for $r \lesssim 3 r_h$ where r_h is the halo radius. Analytic expressions for the dispersion velocity and the pressure are derived yielding at each halo point an ideal DM gas equation of state with local temperature $T(r) \equiv m v^2(r)/3$. $T(r)$ turns to be constant in the same region where the distribution function is thermal. The DM halo can be consistently considered at local thermal equilibrium with: (i) a constant temperature for $r \lesssim 3 r_h$, (ii) a space dependent temperature $T(r)$ for $3 r_h < r \lesssim R_{virial}$, which slowly decreases with r . That is, the DM halo is realistically a self-gravitating thermal gas for $r \lesssim R_{virial}$. $T(r)$ outside the halo radius nicely follows the decrease of the circular velocity squared. When observational data on density profiles of smaller (dwarf) galaxies will become available, the analytic framework provided here will allow to find the phase-space distribution function $f(E)$ for such compact galaxies.

Contents

I. INTRODUCTION	2
II. The Eddington equation for Dark Matter in Galaxies	4
A. Velocity dispersion and Equation of state	6
B. The distribution function behaviour near the halo center for cored profiles	7
C. The distribution function behaviour near the halo center for cusped profiles	8
III. The DM Distribution Function in Galaxies from Empirical halo cored density profiles	10
A. The Galaxy Halo Mass and Scaling Relations	12
B. The Dark Matter Potential Energy	13
C. The resulting distribution function from the Eddington equation turns to be locally thermal.	13
D. The Pauli bound on the distribution function	17
IV. The Halo Dark Matter equation of state	17
A. Polytropic behaviour of the equation of state	18
V. Galaxy Halos turn to be in approximate Local Thermal Equilibrium	19
Acknowledgments	22
VI. Appendix	22

*Electronic address: devega@lpthe.jussieu.fr

†Electronic address: Norma.Sanchez@obspm.fr

I. INTRODUCTION

Dark matter (DM) is the main component of galaxies: the fraction of DM over the total galaxy mass goes from 95% for large diluted galaxies till 99.99% for dwarf compact galaxies. Therefore, DM alone should explain the main structure of galaxies. Baryons should only give corrections to the pure DM results. Astronomical observations show that the DM galaxy density profiles are **cored** till scales below the kpc [1–3].

A central quantity to derive in galaxy structure is the DM chemical potential $\mu(\mathbf{r})$, which is the free energy per particle.

For self-gravitating systems as the DM galaxy halo, the DM chemical potential $\mu(\mathbf{r})$ is proportional to the gravitational potential $\phi(\mathbf{r})$, $\mu(\mathbf{r}) = \mu_0 - m \phi(\mathbf{r})$, μ_0 being a constant, and obeys the **self-consistent** and **nonlinear** Poisson equation

$$\nabla^2 \mu(\mathbf{r}) = -4 \pi g m \rho(\mathbf{r}) = -4 \pi g G m^2 \int \frac{d^3 p}{(2 \pi \hbar)^3} f \left(\frac{p^2}{2m} - \mu(\mathbf{r}) \right). \quad (1.1)$$

Here G is Newton's gravitational constant, g is the number of internal degrees of freedom of the DM particle, p is the DM particle momentum and $f(E)$ is the DM energy distribution function.

In refs. [6, 7, 15, 16] we proposed and developed the Thomas-Fermi approach to galaxy structure for self-gravitating fermionic warm DM (WDM). Given the distribution function $f(E)$, this approach allows to obtain self-consistently the potential $\mu(\mathbf{r})$ from eq.(1.1), as well as the density profiles, velocity dispersion and the equation of state.

In the present paper our aim is to gain knowledge on the central object describing halos: the DM distribution function $f(E)$. For this purpose, instead to compute the density profiles and galaxy relevant structural magnitudes from a given distribution function $f(E)$, we **find** here the distribution function $f(E)$, and the corresponding equation of state, from the observed (empirical) DM halo density profiles $\rho(r)$. Namely, we determine and solve for DM in galaxies the Eddington equation originally used for the gas of stars in globular clusters. The observed density profiles are good realistic starting points and the distribution functions derived from them are realistic ones.

No assumption is made here about the mass of the DM particle, the formalism developed in this paper applies to any kind of DM. In any case, all our results are consistent with a DM particle mass in the keV scale (WDM).

We do not assume any equation of state but we derive and compute it from the distribution function with the general kinetic theory expression [4, 6, 7]

$$P(r) = \frac{1}{3} v^2(r) \rho(r),$$

where $P(r)$ is the pressure.

The short distance behaviour of the density profile determines through the solution of the Eddington equation the behaviour of the distribution function $f(E)$ for the lowest possible energy E . We explicitly compute $f(E)$ for the lowest possible energy both for cored and cusped density profiles. For cored profiles only the quadratic behaviour for small distances:

$$\rho(r) \stackrel{r \rightarrow 0}{\approx} \rho(0) - K r^2, \quad (1.2)$$

where K is a positive constant, provides a physical meaningful distribution function near the center, namely, a positive and bounded distribution function $f(E)$ for the lowest energy E .

For cusped profiles the distribution function always diverges near the halo center.

The distribution function for spin-1/2 fermions must be everywhere smaller than two because of the Pauli principle. Cored density profiles with the behaviour eq.(1.2) satisfy the Pauli bound while cusped profiles always violate the Pauli principle near the halo center.

We explicitly compute the phase-space distribution function and the equation of state for the family of α -density profiles

$$\rho(r) = \frac{\rho_0}{\left[1 + \left(\frac{r}{r_h} \right)^2 \right]^\alpha}, \quad 1 \leq \alpha \leq 2.5. \quad (1.3)$$

This cored density profile is a generalization of the pseudo-thermal profile and with $\alpha \sim 1.5$, it is perfectly appropriate to fit galaxy observations.

For $\alpha \sim 1.5$, we find that inside the halo radius $r < r_h$, the ratio

$$\frac{P(r)}{\rho(r)} = \frac{1}{3} v^2(r)$$

turns to be **approximately constant** (independent of r). Therefore, the local temperature

$$T(r) \equiv \frac{1}{3} m v^2(r) \quad (1.4)$$

is **approximately constant** $T(r) \simeq T_0$ inside the halo radius as shown by figs. 6 and 8. Moreover, this implies that the dark matter obeys locally, at each point of the halo, the ideal gas equation of state

$$P(r) = \frac{T(r)}{m} \rho(r) . \quad (1.5)$$

Furthermore, the distribution function turns to be Boltzmann-like in the region $0 \leq r \lesssim 3 r_h$ with the same temperature T_0 that in the equation of state eq.(1.5) showing the consistency of the thermalization.

In summary, on the basis of galaxy observations, mainly of the galaxy density profiles, and without any assumption about the DM particle mass, we find that the DM in the galaxy halos is approximately thermalized for $r \lesssim 3 r_h$. That is, the DM is a self-gravitating thermal gas in a region extending beyond the halo radius although much smaller than the virial radius R_{virial} .

In the region $3 r_h < r \lesssim R_{virial}$, DM is a virialized self-gravitating gas which can be consistently considered at local thermal equilibrium with a space dependent temperature $T(r)$ that slowly decreases with the distance to the center r as shown in fig. 8.

We introduce the circular temperature $T_c(r)$ associated to the circular velocity in the same way that the temperature $T(r)$ is associated to the velocity through eq.(1.4). We find that the local temperature profile $T(r)$ nicely **follows** the decrease of the circular temperature $T_c(r)$ in the region $r \gtrsim r_h$ as shown in fig. 8.

Physically, these phenomena are clearly understood because in the inner halo region $r \lesssim r_h$, the density is higher than beyond the halo radius. The gravitational interaction in the inner region is strong enough and thermalizes the self-gravitating gas of DM particles while beyond the halo radius the particles are too dilute to thermalize, namely, although they are virialized, they had not enough time to accomplish thermalization. Notice that virialization always starts before than thermalization [18].

In the process of thermalization there is a transfer flow of potential energy into kinetic energy [18]. Clearly, in the outside region $r \gtrsim 3 r_h$ which is only thermalized at the local level, we find that the kinetic energy is lower and therefore the local temperature is lower, than the temperature in the inside the region $r < r_h$ where thermalization is already achieved.

This treatment applies to dilute large galaxies which are in a classical physics regime for halo masses $M_h > 10^6 M_\odot$.

For smaller (dwarf) galaxies there is not yet available information on density profiles from observations. Knowing the density profiles for dwarf galaxies will allow to apply the framework provided in this paper to find the phase-space distribution function $f(E)$ and the velocity dispersion $v^2(r)$ for dwarf galaxies.

On the other hand, the Thomas-Fermi approach to galaxy structure applies to all types of galaxies and allows to determine theoretically all physical magnitudes for them [6]-[7]. It must be noticed that in the classical regime, for halo masses $M_h > 10^6 M_\odot$, the galaxy equation of state computed in the Thomas-Fermi approach yields the same results as found here from the empirical α -profiles and the Eddington equation, namely the Boltzmann self-gravitating gas, showing the robustness of these results.

For dwarf galaxies, the equation of state derived in the Thomas-Fermi theory exhibits deviations from the Boltzmann ideal gas equation of state due to macroscopic quantum effects well accounted by the Thomas-Fermi approach [6]-[7] and which reflect the quantum fermion state near degeneration characteristic of dwarf compact galaxies.

The density profile eq.(1.3) for $\alpha = 2.5$ is not appropriate to describe DM halos but corresponds to the Plummer profile describing the density of stars in globular clusters [10, 11]. We find that the distribution function for the Plummer profile is approximately thermal only for a small range around the center. That is, stars in globular clusters are approximately thermal in a narrower region both in energy and coordinates than the DM in galaxy halos.

We provide here an unified framework in which galaxy structure is obtained from the self-gravitating gas of DM particles in the same way that the globular cluster structure is obtained from a gas of stars.

This paper is organized as follows. In Section 2 we solve the Eddington equation for Dark Matter in Galaxies, we express the velocity dispersion and the pressure in terms of the density profile and compute the distribution function behaviour near the center in cored and cusped profiles. In section 3 we explicitly compute the distribution function for the family of α -density profiles eq.(1.3) showing the approximate thermalization inside the halo radius for $\alpha \sim 1.5$. In section 4 we compute the DM equation of state and confirm the approximate thermalization inside the halo radius. In section 5 we show that the DM outside the halo radius is in local thermal equilibrium with a local temperature slowly decreasing with r .

II. THE EDDINGTON EQUATION FOR DARK MATTER IN GALAXIES

We consider DM dominated galaxies in their late stages of structure formation when they are relaxing to a stationary situation, at least inside the virial radius.

This is a realistic situation since the free-fall (Jeans) time t_{ff} for galaxies is much shorter than the age of galaxies:

$$t_{ff} = \frac{1}{\sqrt{G \rho_0}} = 1.49 \cdot 10^7 \sqrt{\frac{M_\odot}{\rho_0 \text{ pc}^3}} \text{ yr} .$$

The observed central densities of galaxies yield free-fall times in the range from 15 million years for ultra-compact galaxies till 330 million years for large diluted spiral galaxies. These free-fall (or collapse) times are small compared with the age of galaxies running in billions of years.

Hence, we can consider the DM described by a time independent and non-relativistic energy distribution function $f(E)$, where $E = p^2/(2m) - \mu$ is the single-particle energy, m is the mass of the DM particle and μ is the chemical potential [6, 7] related to the gravitational potential $\phi(\mathbf{r})$ by

$$\mu(\mathbf{r}) = \mu_0 - m \phi(\mathbf{r}) , \quad (2.1)$$

where μ_0 is a constant.

It is known from observations that the angular momentum of DM halos is small and therefore DM halos can be considered spherically symmetric. Hence, their phase-space distribution function is only a function of the energy. The methods of this paper could be generalized to anisotropic distributions in which case the distribution function will depend on the angular momentum too [11, 12] but we will not consider it in this paper.

The mass density $\rho(\mathbf{r})$ is expressed as a function of the chemical potential $\mu(\mathbf{r})$ through the standard integral of the DM phase-space distribution function over the momentum

$$\rho(\mathbf{r}) = \frac{g m}{2 \pi^2 \hbar^3} \int_0^\infty dp p^2 f \left[\frac{p^2}{2m} - \mu(\mathbf{r}) \right] , \quad (2.2)$$

where g is the number of internal degrees of freedom of the DM particle, with $g = 1$ for Majorana fermions and $g = 2$ for Dirac fermions. For definiteness, we will take $g = 2$ in the sequel.

The Poisson equation for the gravitational potential $\phi(r)$ takes the self-consistent form

$$\frac{d^2 \mu}{dr^2} + \frac{2}{r} \frac{d\mu}{dr} = -4\pi G m \rho(r) = -\frac{4 G m^2}{\pi \hbar^3} \int_0^\infty dp p^2 f \left[\frac{p^2}{2m} - \mu(r) \right] , \quad (2.3)$$

where G is Newton's constant and we used eq.(2.1).

It is useful to introduce dimensionless variables q , $\nu(q)$

$$r = r_h q \quad , \quad \mu(r) = T_0 \nu(q) \quad , \quad f(E) = \Psi(E/T_0) , \quad (2.4)$$

where we define the core size r_h of the halo by analogy with the Burkert density profile as

$$\frac{\rho(r_h)}{\rho(0)} = \frac{1}{4} . \quad (2.5)$$

T_0 is the characteristic one-particle energy scale. T_0 plays the role of an effective temperature scale and depends on the galaxy mass.

We consider the density profile

$$\rho(r) = \rho_0 F\left(\frac{r}{r_h}\right) = \rho_0 F(q) \quad , \quad \rho_0 \equiv \rho(0) \quad , \quad (2.6)$$

where the given function $F(q)$ takes a bounded value at the origin $F(0) = 1$. That is, we typically consider cored density profiles although our treatment applies for any density profile.

Then, in dimensionless variables the Poisson's equation eq.(2.3) takes the form

$$\frac{d^2\nu}{dq^2} + \frac{2}{q} \frac{d\nu}{dq} = -b_0 F(q) \quad , \quad b_0 \equiv 4 \pi G \rho_0 r_h^2 \frac{m}{T_0} \quad . \quad (2.7)$$

This equation can be solved in closed form with the solution

$$\nu(q) = \nu(0) - b_0 \int_0^q \left(1 - \frac{q'}{q}\right) q' F(q') dq' \quad , \quad \frac{d\nu}{dq} = -\frac{b_0}{q^2} \int_0^q q'^2 F(q') dq' \quad . \quad (2.8)$$

In dimensionless variables, for spherically symmetric distributions, eq.(2.2) becomes

$$\rho(r) = \frac{\sqrt{2}}{\pi^2} m^{\frac{5}{2}} T_0^{\frac{3}{2}} \int_{\nu(\infty)}^{\nu} d\nu' \sqrt{\nu - \nu'} \Psi(-\nu') \quad , \quad \nu' \equiv \nu - \frac{p^2}{2mT_0} \quad . \quad (2.9)$$

$\nu(q)$ takes its minimum value at $q = \infty$. This is so because $d\nu(q)/dq < 0$ as follows from eq.(2.8). Therefore, this minimum value $\nu(\infty)$ is the lower bound of integration in ν' . The chemical potential for galaxies is always negative except for the dwarf compact galaxies in the quantum regime [16]. Hence, $\nu(\infty)$ is always negative except in the limiting case of degenerate WDM fermions [16].

Eq.(2.9) can thus be written as

$$F(\nu) = \frac{\sqrt{2}}{\pi^2} \frac{m^{\frac{5}{2}} T_0^{\frac{3}{2}}}{\rho_0} \int_{\nu(\infty)}^{\nu} d\nu' \sqrt{\nu - \nu'} \Psi(-\nu') \quad . \quad (2.10)$$

Eq.(2.10) expressing the density profile in terms of the distribution function is the *Abel integral* equation and can be explicitly inverted as [8],

$$\Psi(-\nu) = \sqrt{2} \pi \frac{\rho_0}{m^{\frac{5}{2}} T_0^{\frac{3}{2}}} \int_{\nu(\infty)}^{\nu} \frac{d\nu'}{\sqrt{\nu - \nu'}} \frac{d^2 F}{d\nu'^2} \quad , \quad (2.11)$$

with Ψ and $d\Psi/d\nu$ vanishing at infinite distance $q = \infty$ as boundary condition.

Eq.(2.11) is the *Eddington formula*, originally derived for a gas of stars forming a globular cluster [9]. However, here, we have eq.(2.11) for a gas of DM particles forming the galaxy halo. Given the density profile $F(q)$, the distribution function $\Psi(-\nu)$ follows by quadratures.

It is useful to re-scale the potential $\nu(q)$ as

$$\nu(q) = \nu(0) + b_0 \varepsilon(q) \quad , \quad (2.12)$$

with the coefficient b_0 given by eq.(2.7). Then, eq.(2.8) yields

$$\varepsilon(q) = - \int_0^q \left(1 - \frac{q'}{q}\right) q' F(q') dq' \quad , \quad \frac{d\varepsilon}{dq} = -\frac{1}{q^2} \int_0^q q'^2 F(q') dq' \quad , \quad \varepsilon(0) = 0 \quad . \quad (2.13)$$

$\varepsilon(q)$ is related to the potential energy $E(q)$ of a particle at the point q in the galaxy by

$$E(q) = E(0) - 4 \pi G \rho_0 r_h^2 m \varepsilon(q)$$

Hence, $-\varepsilon(q)$ is the particle potential energy in units of $4 \pi G \rho_0 r_h^2 m$ taking as reference the potential energy at the origin.

Since the profile F is given explicitly as a function of q , it is convenient in eq.(2.11) to change the integration variable from ν' to q' using eqs.(2.12)-(2.13) with the result

$$\Psi(q) = \frac{1}{G^{\frac{3}{2}} r_h^3 m^4 \sqrt{\rho_0}} \mathcal{D}(q) \quad , \quad \mathcal{D}(q) \equiv \frac{1}{\sqrt{32} \pi} \int_q^\infty \frac{\mathcal{J}(q') dq'}{\sqrt{\varepsilon(q) - \varepsilon(q')}} \quad (2.14)$$

$$\text{where} \quad \mathcal{J}(q) \equiv \frac{1}{\left(-\frac{d\varepsilon}{dq}\right)} \left[\frac{d^2 F}{dq^2} - \frac{\frac{d^2 \varepsilon}{dq^2}}{\frac{d\varepsilon}{dq}} \frac{dF}{dq} \right] \quad (2.15)$$

Notice that from eq.(2.13) $\left(-\frac{d\varepsilon}{dq} > 0\right)$.

Inserting in the integral of eq.(2.14) a given expression for the density profile $F(q)$ and the dimensionless gravitational potential $-\varepsilon(q)$ computed from eq.(2.13) allows to obtain the corresponding distribution function Ψ .

The coefficient in front of $\mathcal{D}(q)$ in eq.(2.14) can be evaluated as

$$\frac{1}{G^{\frac{3}{2}} r_h^3 m^4 \sqrt{\rho_0}} = 0.502753 \times 10^{-5} \left(\frac{2 \text{ keV}}{m}\right)^4 \left(\frac{\text{kpc}}{r_h}\right)^{\frac{5}{2}} \sqrt{\frac{120 M_\odot}{\Sigma_0 \text{ pc}^2}} \quad (2.16)$$

A. Velocity dispersion and Equation of state

The average velocity dispersion of the particles depends on r and follows from the average momentum as

$$v^2(r) = \frac{1}{m^2} \frac{\int_0^\infty p^4 dp f \left[\frac{p^2}{2m} - \mu(r) \right]}{\int_0^\infty p^2 dp f \left[\frac{p^2}{2m} - \mu(r) \right]} = \frac{2 T_0}{m} \frac{\int_{\nu(\infty)}^\nu d\nu' [\nu(q) - \nu']^{\frac{3}{2}} \Psi(-\nu')}{\int_{\nu(\infty)}^\nu d\nu' \sqrt{\nu(q) - \nu'} \Psi(-\nu')} \quad (2.17)$$

From eq.(2.10) the denominator here is proportional to the density profile and we obtain

$$v^2(r) = \frac{2\sqrt{2}}{\pi^2} \frac{m^{\frac{3}{2}} T_0^{\frac{5}{2}}}{\rho_0 F(q)} \int_{\nu(\infty)}^\nu d\nu' [\nu(q) - \nu']^{\frac{3}{2}} \Psi(-\nu') \quad (2.18)$$

We compute this integral in the Appendix A with the result

$$\int_{\nu(\infty)}^\nu d\nu' (\nu - \nu')^{\frac{3}{2}} \Psi(-\nu') = \frac{3\pi^2}{4\sqrt{2}} \frac{\rho_0}{m^{\frac{5}{2}} T_0^{\frac{3}{2}}} \int_{\nu(\infty)}^\nu d\nu' (\nu - \nu')^2 \frac{d^2 F}{d\nu'^2} \quad (2.19)$$

Inserting this expression in eq.(2.18) yields the velocity dispersion in terms of the density profile

$$v^2(r) = \frac{3 T_0}{2 m F(q)} \int_{\nu(\infty)}^\nu d\nu' [\nu(q) - \nu']^2 \frac{d^2 F}{d\nu'^2} \quad (2.20)$$

As above, it is convenient to change the integration variable from ν' to q' with the result

$$v^2(r) = 6 \pi G \rho_0 r_h^2 \frac{1}{F(q)} \int_q^\infty dq' [\varepsilon(q) - \varepsilon(q')]^2 \mathcal{J}(q') \quad (2.21)$$

where $\mathcal{J}(q)$ is given by eq.(2.15). From eq.(2.6) and eq.(2.21) we can immediately compute the pressure in terms of the density profile $F(q)$ as

$$P(r) = \frac{1}{3} v^2(r) \rho(r) \quad (2.22)$$

$$P(r) = 2 \pi G \Sigma_0^2 \int_q^\infty dq' [\varepsilon(q) - \varepsilon(q')]^2 \mathcal{J}(q') \quad , \quad \Sigma_0 \equiv \rho_0 r_h \quad (2.23)$$

where Σ_0 is the surface density.

It must be noticed that the surface density Σ_0 is found nearly **constant** and independent of luminosity in different galactic systems (spirals, dwarf irregular and spheroidals, elliptics) spanning over 14 magnitudes in luminosity and over different Hubble types. More precisely, all galaxies seem to have the same value for Σ_0 , namely $\Sigma_0 \simeq 120 M_\odot/\text{pc}^2$ up to 10% – 20% [20–22]. It is remarkable that at the same time other important structural quantities as r_h , ρ_0 , the baryon-fraction and the galaxy mass vary orders of magnitude from one galaxy to another.

Given the profile function $F(q)$, and so the density $\rho(r)$ from eq.(2.6), we determine the pressure $P(r)$ from eq.(2.22). In this way, we can find the relation between pressure and density associating to each value of $\rho(r)$ the corresponding value $P(r)$. We thus obtain the equation of state as a numerical table.

In subsections IV and IV A below we compute and analyze the halo DM equation of state and plot it in figs. 6 and 7.

The hydro-static equilibrium equation

$$\frac{dP}{dr} + \rho(r) \frac{d\phi}{dr} = 0, \quad (2.24)$$

is satisfied here as in the case of the Thomas-Fermi theory [6, 7, 15, 16].

B. The distribution function behaviour near the halo center for cored profiles

The lowest energy $-\varepsilon(q)$ for a DM particle in the galaxy halo occurs near the center $q = 0$. We derive in this subsection the behaviour of the distribution function for $q \rightarrow 0$ from the behaviour of cored profile functions $F(q)$ near the center using the explicit formula eq.(2.14).

For a cored density profile approaching the center as a power of the coordinate we have in general

$$F(q) \stackrel{q \rightarrow 0}{\simeq} 1 - c q^\beta, \quad \beta > 0, \quad (2.25)$$

where c and β are positive constants.

For a Burkert profile

$$F(q) = \frac{1}{(q+1)(q^2+1)},$$

and we have $c = \beta = 1$.

A Einasto or Sersic profile can be parametrized as

$$F(q) = \exp(-q^\beta)$$

and we have for galaxies $c = 1$ and typically $\beta \sim 0.4$.

Density profiles obtained from primordial density fluctuations [5] as well as from the Thomas-Fermi approach [6, 7] are even functions of r and exhibit at small distances the behaviour eq.(2.25) with $\beta = 2$.

From eq.(2.13) we find for the particle energy $-\varepsilon(q)$ near the center

$$-\varepsilon(q) \stackrel{q \rightarrow 0}{\simeq} \frac{q^2}{6} \left[1 - \frac{6c}{(\beta+2)(\beta+3)} q^\beta \right]. \quad (2.26)$$

Inserting eqs.(2.25) and (2.26) in the dimensionless distribution function eq.(2.14) yields

$$\mathcal{D}(q) \stackrel{q \rightarrow 0}{\simeq} \frac{3\sqrt{3}}{4\sqrt{\pi}} c \beta (2-\beta) \int_q^\infty \frac{q'^{\beta-3} dq'}{\sqrt{q'^2 - q^2}} = \frac{3}{8} \sqrt{3} c \beta (2-\beta) \frac{\Gamma\left(\frac{3-\beta}{2}\right)}{\Gamma\left(2-\frac{\beta}{2}\right)} \frac{1}{q^{3-\beta}} \quad (2.27)$$

This dimensionless distribution function behaviour can be expressed in terms of the particle energy $-\varepsilon(q)$ with the result

$$\mathcal{D}(-\varepsilon) \stackrel{\varepsilon \rightarrow 0}{\cong} \frac{c \beta}{8 \sqrt{2}} \frac{\Gamma\left(\frac{3-\beta}{2}\right)}{\Gamma\left(1-\frac{\beta}{2}\right)} \frac{1}{(-\varepsilon)^{\frac{3-\beta}{2}}}. \quad (2.28)$$

We see that for β in the interval $0 < \beta < 3$, the distribution function diverges for the lowest energy $\varepsilon \rightarrow 0$ except if $\beta = 2$.

In addition, from eqs.(2.27)-(2.28) we find that $\mathcal{D}(-\varepsilon)$ for $\varepsilon \rightarrow 0$ becomes negative (i. e. unphysical) for β in the interval:

$$2l + 1 > \beta > 2l \quad , \quad l = 1, 2, 3, \dots$$

The case $\beta = 2l$, $l = 1, 2, 3, \dots$ is special. For $\beta = 2l$ we have

$$\left. \frac{1}{\Gamma\left(1-\frac{\beta}{2}\right)} \right|_{\beta=2l} = 0 \quad , \quad l = 1, 2, 3, \dots$$

and the leading contribution to $\mathcal{D}(-\varepsilon)$ in eqs.(2.27)-(2.28) identically vanishes.

Analyzing the $q \rightarrow 0$ behaviour of the integrand of eq.(2.14) we find that $\mathcal{D}(0)$ is **finite and positive** when $\beta = 2l$, $l = 1, 2, 3, \dots$. From eq.(2.25) this implies that physically reasonable density profiles behave for $q \rightarrow 0$ as

$$F(q) \stackrel{q \rightarrow 0}{\cong} 1 - c q^{2l} \quad , \quad l \geq 1. \quad (2.29)$$

However, a leading $q \rightarrow 0$ behaviour q^{2l} with $l > 1$ describe non-generic density profiles where even powers of q smaller than q^{2l} are missing.

In summary, only remains the case $l = 1$ and hence $\beta = 2$ in eq.(2.25) describes the generic density profile which provides **finite and positive** distribution functions near the halo center:

$$F(q) \stackrel{q \rightarrow 0}{\cong} 1 - c q^2 \quad (2.30)$$

From now on we shall only consider this cored density profile behaviour ($\beta = 2$).

We have seen how the analysis of the distribution function near the halo center allows to select physically meaningful density profiles.

The distribution function for spin-1/2 fermions must be everywhere smaller than two in order to satisfy the Pauli principle. Cored density profiles with the behaviour eq.(2.30) satisfy the Pauli bound as we discuss below in sec. III D.

C. The distribution function behaviour near the halo center for cusped profiles

The generic behaviour of a cusped density profile near the center $q = 0$ is a power-like singularity

$$F(q) \stackrel{q \rightarrow 0}{\cong} \frac{\mathcal{C}}{q^\lambda} \quad , \quad \lambda < 3 \quad (2.31)$$

where \mathcal{C} and λ are positive constants. λ must be smaller than 3 to have finite mass.

For the NFW profile we have $\lambda = 1$ and for the Jaffe profile we have $\lambda = 2$ [11].

From eq.(2.13) we find for the particle energy $-\varepsilon(q)$ near the center

$$-\varepsilon(q) \stackrel{q \rightarrow 0}{\cong} \frac{\mathcal{C}}{(3-\lambda)(2-\lambda)} q^{2-\lambda} \quad , \quad 0 < \lambda < 3, \lambda \neq 2. \quad (2.32)$$

For $\lambda = 2$ we obtain

$$-\varepsilon(q) \stackrel{q \rightarrow 0}{\approx} \mathcal{C} \ln q + c_1 \rightarrow +\infty \quad (2.33)$$

where c_1 is a constant. We see that

$$\lim_{q \rightarrow 0} \varepsilon(q) = \begin{cases} 0 & \text{for } 0 < \lambda < 2, \\ +\infty & \text{for } 2 \leq \lambda < 3. \end{cases}$$

Inserting eqs.(2.31) and (2.32) in the dimensionless distribution function eq.(2.14) yields near the center

$$\mathcal{D}(q) \stackrel{q \rightarrow 0}{\approx} \lambda (3 - \lambda)^{\frac{3}{2}} \sqrt{\frac{2 - \lambda}{8 \pi \mathcal{C}}} \int_q^\infty \frac{dq'}{\sqrt{q'^{2-\lambda} - q^{2-\lambda}}} = \frac{\lambda (3 - \lambda)^{\frac{3}{2}}}{\sqrt{8 \mathcal{C}(2 - \lambda)}} \frac{\Gamma\left(\frac{1}{2} + \frac{2}{2 - \lambda}\right)}{\Gamma\left(1 + \frac{2}{2 - \lambda}\right)} \frac{1}{q^{3-\lambda/2}} \quad \text{for } 0 < \lambda < 2,$$

$$\mathcal{D}(q) \stackrel{q \rightarrow 0}{\approx} \lambda (3 - \lambda)^{\frac{3}{2}} \sqrt{\frac{\lambda - 2}{8 \pi \mathcal{C}}} \int_q^\infty \frac{dq'}{\sqrt{q'^{2-\lambda} - q'^{2-\lambda}}} = \frac{\lambda (3 - \lambda)^{\frac{3}{2}}}{\sqrt{8 \mathcal{C}(\lambda - 2)}} \frac{\Gamma\left(\frac{2}{\lambda - 2}\right)}{\Gamma\left(\frac{1}{2} + \frac{2}{\lambda - 2}\right)} \frac{1}{q^{3-\lambda/2}} \quad \text{for } 2 < \lambda < 3.$$

which in terms of the particle energy $-\varepsilon(q)$ becomes

$$\mathcal{D}(-\varepsilon) \stackrel{\varepsilon \rightarrow 0}{\approx} \frac{\lambda}{\sqrt{8}} \left[\frac{\mathcal{C}^2}{(3 - \lambda)^\lambda} \right]^{\frac{1}{2-\lambda}} \frac{1}{(2 - \lambda)^{1 + \frac{2}{2-\lambda}}} \frac{\Gamma\left(\frac{1}{2} + \frac{2}{2 - \lambda}\right)}{\Gamma\left(1 + \frac{2}{2 - \lambda}\right)} (-\varepsilon)^{-\frac{1}{2} - \frac{2}{2-\lambda}} \rightarrow +\infty \quad \text{for } 0 < \lambda < 2,$$

$$\mathcal{D}(-\varepsilon) \stackrel{\varepsilon \rightarrow \infty}{\approx} \frac{\lambda}{\sqrt{8}} \left[\frac{(3 - \lambda)^\lambda}{\mathcal{C}^2} \right]^{\frac{1}{\lambda-2}} (\lambda - 2)^{\frac{2}{\lambda-2} - 1} \frac{\Gamma\left(\frac{2}{\lambda - 2}\right)}{\Gamma\left(\frac{1}{2} + \frac{2}{\lambda - 2}\right)} \varepsilon^{\frac{3-\lambda/2}{\lambda-2}} \rightarrow +\infty \quad \text{for } 2 < \lambda < 3. \quad (2.34)$$

We see that for $0 < \lambda < 3$, the distribution function $\mathcal{D}(-\varepsilon)$ **diverges** for the lowest energy: for $\varepsilon \rightarrow 0$ in the case $0 < \lambda < 2$ and for $\varepsilon \rightarrow \infty$ in the case $2 < \lambda < 3$.

For $\lambda = 2$ we obtain from eqs.(2.14), (2.31) and (2.33)

$$\mathcal{D}(q) \stackrel{q \rightarrow 0}{\approx} \frac{1}{\sqrt{2 \pi \mathcal{C}}} \int_q^\infty \frac{dq'}{q'^3 \sqrt{\ln\left(\frac{q'}{q}\right)}} = \frac{1}{\sqrt{2 \mathcal{C}} q^2}, \quad \lambda = 2. \quad (2.35)$$

Therefore, we have in terms of the particle energy $-\varepsilon(q)$

$$\mathcal{D}(-\varepsilon) \stackrel{\varepsilon \rightarrow \infty}{\approx} \frac{1}{\mathcal{C}_2} \exp\left(\frac{2}{\mathcal{C}} \varepsilon\right) \rightarrow +\infty, \quad \lambda = 2. \quad (2.36)$$

where \mathcal{C}_2 is a constant. We see that cusped profiles with $1/q^2$ behavior near the center produce a Boltzmann distribution function for large energies $\varepsilon(q) \rightarrow +\infty$. Thermal behavior only appears near the center in the case $\lambda = 2$. For $\lambda \neq 2$, eqs.(2.34) clearly show a non-Boltzmann behavior for the lowest possible energies.

Cusped density profiles yield distribution functions that **diverge** near the halo center. Clearly, such distribution functions cannot describe spin-1/2 fermions since they violate the Pauli principle near the halo center.

III. THE DM DISTRIBUTION FUNCTION IN GALAXIES FROM EMPIRICAL HALO CORED DENSITY PROFILES

We explicitly compute the phase-space distribution function and the equation of state for the family of α -density profiles

$$F(q) = \frac{1}{(1+q^2)^\alpha} \quad , \quad 1 \leq \alpha \leq 2.5 \quad , \quad q = \frac{r}{r_h} . \quad (3.1)$$

This cored density profile is a generalization of the pseudo-thermal profile and it is perfectly appropriate to fit galaxy observations.

As shown in subsection II B, density profiles with the short distance behaviour eq.(2.30) produce meaningful distribution functions at short distances. The α -density profiles eq.(3.1) fulfil eq.(2.30) at small distances. This is not the case of Burkert, Einasto and Sersic profiles which exhibit divergent distribution functions at short distances [see eqs.(2.27)-(2.28) for $\beta \neq 2$]. For all these reasons we will concentrate from now on the family of density profiles given by eq.(3.1).

An α -density profile eq.(3.1) with $\alpha = 1.5913$ is an excellent approximation to the Thomas-Fermi density profile in the internal region $r \lesssim 3 r_h$ [16].

Observations for all r till the virial radius are best fitted for the values

$$\alpha = 1.2 - 1.5 .$$

In particular, for $q \gg 1$ and $\alpha = 1.5$, eq.(3.1) reproduces the Burkert density profile.

Spiral and elliptic galaxy observations favour the value $\alpha = 1.2$ [14]. Although observations disfavour α values outside the 1.2 - 1.5 range, it is useful and illustrative for the purposes of understanding to analyze the whole range of values $1 < \alpha \leq 2.5$.

The value $\alpha = 2.5$ is not appropriate to describe realistic DM halos but corresponds to the Plummer profile describing the density of stars in globular clusters [10, 11].

For the density profile eq.(3.1), the normalized gravitational potential $\varepsilon(q)$ eq.(2.13) is given by

$$\varepsilon(q) = \frac{w_\alpha(q)}{q} + \frac{1}{2(\alpha-1)} \left[\frac{1}{(1+q^2)^{\alpha-1}} - 1 \right] \quad , \quad \varepsilon(\infty) = -\frac{1}{2(\alpha-1)} \quad , \quad (3.2)$$

$$w_\alpha(q) \equiv \int_0^q \frac{s^2 ds}{(1+s^2)^\alpha} = \frac{q^3}{3} {}_2F_1 \left(\alpha, \frac{3}{2}; \frac{5}{2}; -q^2 \right) \quad , \quad (3.3)$$

where ${}_2F_1(a, b; c; z)$ stands for the hypergeometric function [17]. At fixed q , $w_\alpha(q)$ monotonically decreases when α grows.

In the particular cases $\alpha = 1, \frac{3}{2}, 2, \frac{5}{2}$ the function $w_\alpha(q)$ reduces to elementary functions [13]:

$$\begin{aligned} w_1(q) &= q - \arctan q \quad , \quad \varepsilon(q) = 1 - \frac{\arctan q}{q} - \frac{1}{2} \ln(1+q^2) \quad , \quad \alpha = 1 \quad , \\ w_{\frac{3}{2}}(q) &= \text{Arg Sinh}(q) - \frac{q}{\sqrt{1+q^2}} \quad , \quad \varepsilon(q) = \frac{\text{Arg Sinh}(q)}{q} - 1 \quad , \quad \alpha = \frac{3}{2} \quad , \\ w_2(q) &= \frac{q}{2} \left(\frac{\arctan q}{q} - \frac{1}{1+q^2} \right) \quad , \quad \varepsilon(q) = -\frac{1}{2} \left(1 - \frac{\arctan q}{q} \right) \quad , \quad \alpha = 2 \quad , \\ w_{\frac{5}{2}}(q) &= \frac{q^3}{3(1+q^2)^{\frac{3}{2}}} \quad , \quad \varepsilon(q) = -\frac{1}{3} \left(1 - \frac{1}{\sqrt{1+q^2}} \right) \quad , \quad \alpha = \frac{5}{2} \quad . \end{aligned} \quad (3.4)$$

We plot in fig. 1 the dimensionless energy $-\varepsilon(q)$ as a function of $\log_{10} q$ for relevant values of the exponent α in the density profile eq.(3.1). We see that $-\varepsilon(q)$ grows monotonically with q . Small energy values $-\varepsilon(q) \lesssim 0.1$ are confined inside the halo radius $r \lesssim r_h$, i. e. $q \lesssim 1$.

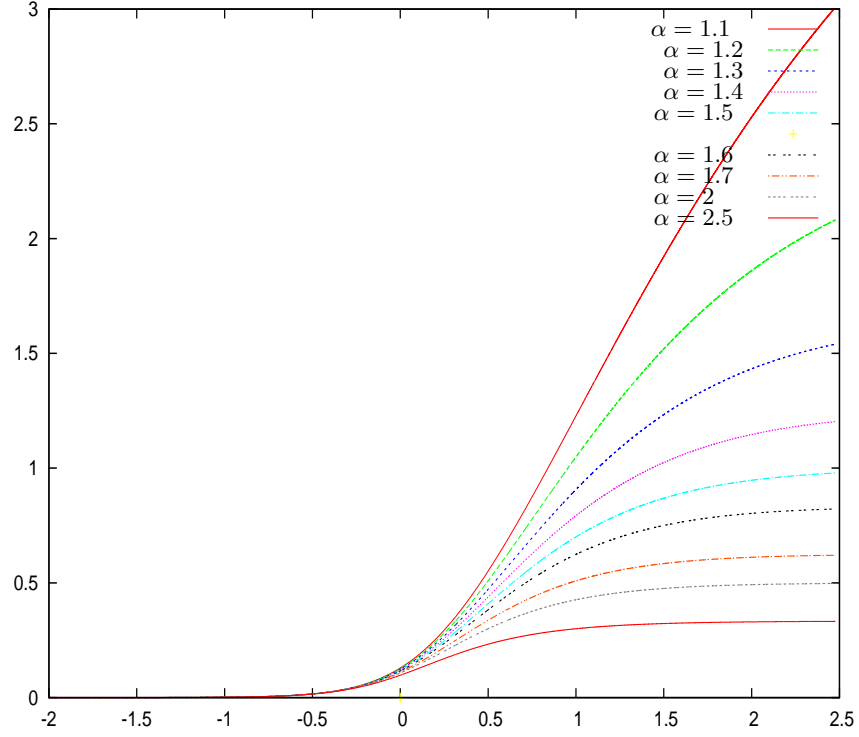


FIG. 1: The dimensionless energy $-\varepsilon(q)$ given by eq.(3.2) vs. the ordinary logarithm of the coordinate $q = r/r_h$ for relevant values of the exponent α in the density profile eq.(3.1). For increasing q , $-\varepsilon(q)$ increases slowly. Notice the **shallow** potential felt by the particles inside the halo for $r < r_h$, $\log_{10} q < 0$.

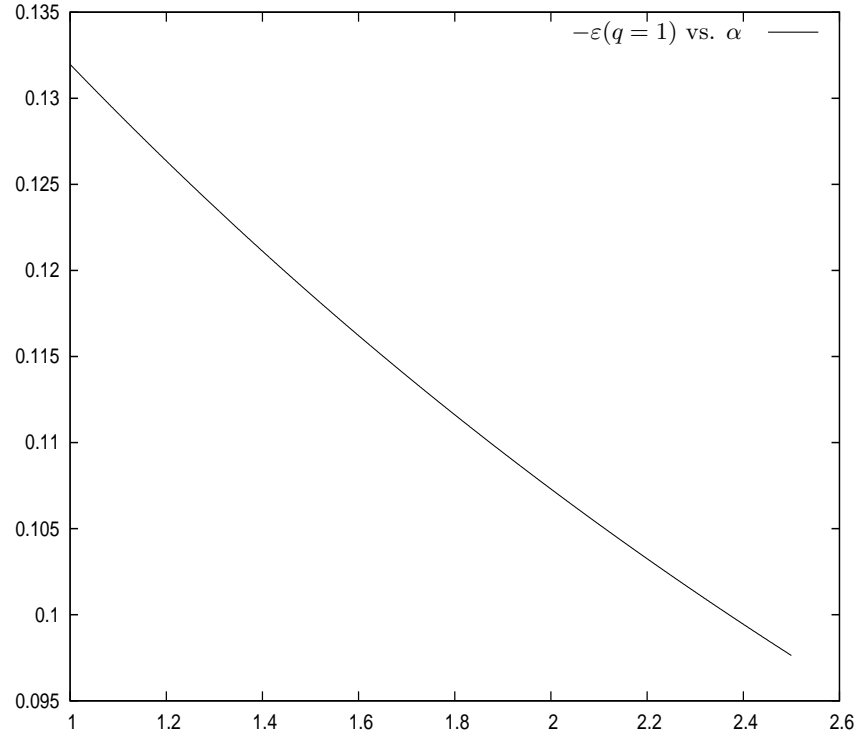


FIG. 2: The dimensionless energy at the halo radius $r = r_h$, $-\varepsilon(1)$ vs. the exponent α in the density profile eq.(3.1). $-\varepsilon(q = 1)$ turns to be near 0.1 in the whole range $1 < \alpha < 2.5$. That is, the potential energy of a particle is quite small inside the halo, $q < 1$.

We plot in fig. 2 the energy at the halo radius $r = r_h$, $-\varepsilon(q = 1)$ as a function of α in the interval $1 < \alpha < 2.5$. We see that $-\varepsilon(1) \simeq 0.1$ in this range. In particular, $-\varepsilon(1) = 0.118626$ for $\alpha = \frac{3}{2}$.

As a consequence, only particles with $-\varepsilon(q) \lesssim 0.1$ stay inside the halo $r < r_h$. $-\varepsilon(q)$ grows slowly when the distance to the origin q grows. For example, $-\varepsilon(10) = 0.700178$ for $\alpha = \frac{3}{2}$ as shown in fig. 1.

A. The Galaxy Halo Mass and Scaling Relations

The dark matter mass inside a radius R follows by integrating the mass density eqs.(2.6) and (3.1)

$$M(r) = 4 \pi \int_0^r r'^2 dr' \rho(r') = 4 \pi \rho_0 r_h^3 w_\alpha(q) . \quad (3.5)$$

For $r \rightarrow \infty$, $M(r)$ has a bounded limit for $\alpha > \frac{3}{2}$. The $q = \infty$ limit of $w_\alpha(q)$ follows from eqs.(3.3) with the result[17]

$$w_\alpha(\infty) = \frac{\sqrt{\pi}}{4} \frac{\Gamma(\alpha - \frac{3}{2})}{\Gamma(\alpha)} , \quad \alpha > \frac{3}{2} .$$

We find in the particular cases $\alpha = 2, \frac{5}{2}$

$$w_2(\infty) = \frac{\pi}{4} , \quad w_{\frac{5}{2}}(\infty) = \frac{1}{3} .$$

The halo mass M_h follows by setting here $r = r_h$ (i. e. $q = 1$):

$$M_h \equiv M(r_h) = 4 \pi \int_0^{r_h} r^2 dr \rho(r) = d_\alpha \rho_0 r_h^3 , \quad d_\alpha \equiv 4 \pi w_\alpha(1) , \quad (3.6)$$

where $w_\alpha(q = 1)$ is given by eq.(3.3). It follows from eq.(3.3) that $w_\alpha(1)$ is a decreasing function of α .

In the cases $\alpha = 1, \frac{3}{2}, 2, \frac{5}{2}$, d_α takes the values

$$d_1 = \pi(4 - \pi) = 2.696766 , \quad d_{\frac{3}{2}} = 4 \pi \left[\ln(1 + \sqrt{2}) - \frac{1}{\sqrt{2}} \right] = 2.18990$$

$$d_2 = \frac{\pi}{2} (\pi - 2) = 1.793210 , \quad d_{\frac{5}{2}} = \frac{\pi}{3} \sqrt{2} = 1.480961 .$$

We derived in this way the **scaling relation** eq.(3.6). Both the amplitude and exponent in eq.(3.6) are well verified by galaxy observations.

It must be stressed that the Thomas-Fermi (TF) theoretical approach to galaxy structure yields a similar formula to eq.(3.6) for the halo mass M_h of galaxies in the dilute regime ($M_h > 10^6 M_\odot$) [16]

$$M_h = d_{TF} \rho_0 r_h^3 , \quad d_{TF} = 1.75572 .$$

On the other hand, the empiric Burkert profile yields a similar expression for M_h with $d_{Burkert} = 1.59796$ [19].

The slight difference between the coefficients d for the different types of profiles can be retraced from the fact that the shapes of the Thomas-Fermi profile, Burkert profile, and the α -profiles eq.(3.1) are different. Consequently, for a given halo mass M_h , the halo radius eq. (2.5) for these different profiles are different to each other, and the coefficients d are slightly different too.

It is remarkable, however, that all these coefficients d are close to each other indicating the **robustness** of the scaling relation

$$M_h = d \rho_0 r_h^3 = d \Sigma_0 r_h^2 . \quad (3.7)$$

B. The Dark Matter Potential Energy

The dark matter potential energy inside a radius R is given by

$$U(R) = -4 \pi G \int_0^R r dr \rho(r) M(r) .$$

Using eq.(2.6) and eq.(3.5) yields

$$U(R) = -(4 \pi)^2 G \Sigma_0^2 r_h^3 u(Q) , \quad u(Q) \equiv \int_0^Q q dq F(q) w_\alpha(q) , \quad Q \equiv R/r_h . \quad (3.8)$$

At fixed Q , $u(Q)$ monotonically decreases for increasing α .

For $R \rightarrow \infty$, $U(R)$ has a bounded limit for $\alpha > 1.25$. The $Q = \infty$ limit of $u(Q)$ follows from eqs.(3.3) and (3.8) with the result [17]

$$u_\alpha(\infty) = \frac{\sqrt{\pi}}{8(\alpha-1)} \frac{\Gamma(2\alpha - \frac{5}{2})}{\Gamma(2\alpha - 1)} , \quad \alpha > \frac{5}{4} . \quad (3.9)$$

In particular, for $\alpha = \frac{3}{2}$, 2, $\frac{5}{2}$ we have

$$u_{\frac{3}{2}}(\infty) = \frac{\pi}{4} , \quad u_2(\infty) = \frac{\pi}{32} , \quad u_{\frac{5}{2}}(\infty) = \frac{\pi}{96} .$$

C. The resulting distribution function from the Eddington equation turns to be locally thermal.

The distribution function follows by inserting the density profile eq.(3.1) and the potential energy $\varepsilon(q)$ eq.(3.2) in the integral representation eq.(2.14) with the result

$$\Psi(q) = \frac{1}{G^{\frac{3}{2}} r_h^3 m^4 \sqrt{\rho_0}} \mathcal{D}(q) , \quad (3.10)$$

$$\mathcal{D}(q) \equiv \frac{\alpha}{\sqrt{8\pi}} \int_q^\infty \frac{q'^2 dq'}{\sqrt{\varepsilon(q) - \varepsilon(q')}} \frac{1}{w_\alpha^2(q') (1 + q'^2)^{\alpha+2}} \left\{ [(2\alpha - 1) q'^2 - 3] w_\alpha(q') + \frac{q'^3}{(1 + q'^2)^{\alpha-1}} \right\} . \quad (3.11)$$

From eqs.(2.21) and (2.22) we obtain analogous expressions for the velocity dispersion and the pressure

$$v^2(r) = 3 G \Sigma_0 r_h \frac{\Pi(q)}{F(q)} , \quad P(r) = G \Sigma_0^2 \Pi(q) , \quad (3.12)$$

$$\Pi(q) \equiv 4 \pi \alpha \int_q^\infty q'^2 dq' \frac{[\varepsilon(q) - \varepsilon(q')]^2}{w_\alpha^2(q') (1 + q'^2)^{\alpha+2}} \left\{ [(2\alpha - 1) q'^2 - 3] w_\alpha(q') + \frac{q'^3}{(1 + q'^2)^{\alpha-1}} \right\} . \quad (3.13)$$

The hydro-static equilibrium equation eq.(2.24) in dimensionless variables takes the form

$$\frac{d\Pi}{dq} = 4 \pi F(q) \frac{d\varepsilon}{dq} = -4 \pi \frac{F(q)}{q^2} \int_0^q q'^2 F(q') dq' . \quad (3.14)$$

In the particular cases $\alpha = 1, \frac{3}{2}, 2, \frac{5}{2}$ the hydrostatic equilibrium equation eq.(3.14) can be integrated in close form with the following results:

$$\Pi(q) = 4 \pi \left[\frac{\pi^2}{8} - \frac{\arctan q}{q} - \frac{1}{2} (\arctan q)^2 \right] , \quad \alpha = 1 ,$$

$$\Pi(q) = 4 \pi \left[\frac{1}{2(1 + q^2)} + \frac{1 + 2 q^2}{q \sqrt{1 + q^2}} \text{Arg Sinh}(q) - \ln(1 + q^2) - \ln 4 \right] , \quad \alpha = \frac{3}{2} , \quad (3.15)$$

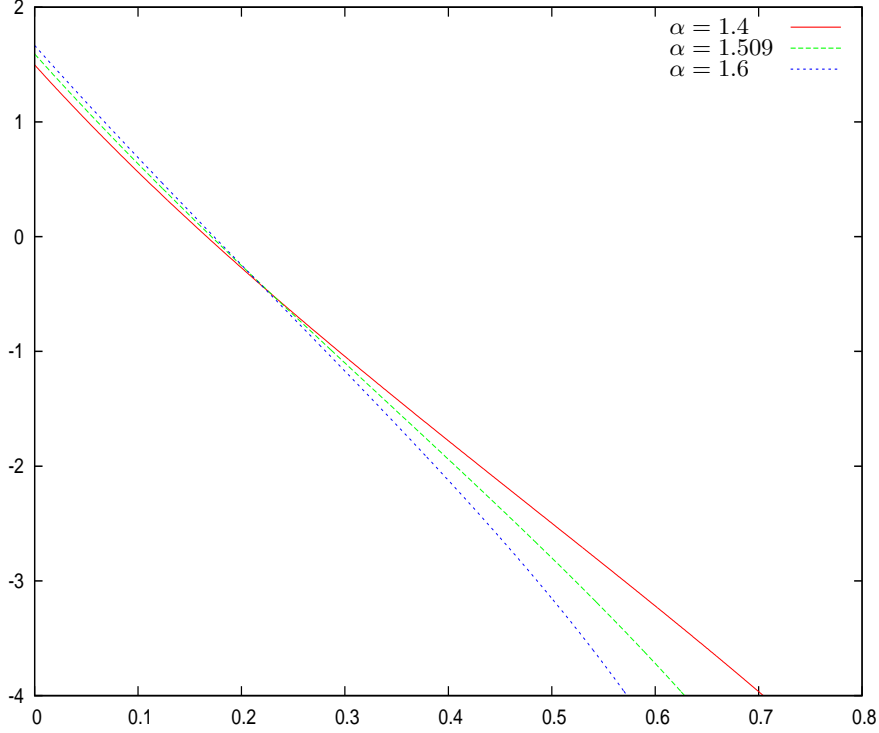


FIG. 3: The natural logarithm of the normalized distribution function $\mathcal{D}(-\varepsilon)$ eq.(3.11) vs. the energy $-\varepsilon$ eq.(3.2) for the values of the exponent α in the density profiles eq.(3.1) $\alpha = 1.4, 1.509$ and 1.6 appropriate for DM halos. Notice the **linear** behaviour of $\ln \mathcal{D}(-\varepsilon)$ indicating an approximately **Boltzman** distribution function $\mathcal{D}(-\varepsilon)$ for $0 \leq -\varepsilon \lesssim 0.7$ and $0 < q \lesssim 7$, i. e. $0 < r \lesssim 7 r_h$.

$$\Pi(q) = \frac{\pi}{2} \left[\frac{3q^2 + 4}{(1 + q^2)^2} + \frac{2(3q^2 + 2)}{q(q^2 + 1)} \arctan q + 3 (\arctan q)^2 - \frac{3}{4} \pi^2 \right] , \quad \alpha = 2 ,$$

$$\Pi(q) = \frac{2\pi}{9} \frac{1}{(1 + q^2)^3} , \quad \alpha = \frac{5}{2} .$$

For the Plummer profile of globular star clusters ($\alpha = \frac{5}{2}$) it follows that a polytropic equation of state is fulfilled exactly

$$\Pi(q) = \frac{2\pi}{9} F^{\frac{6}{5}}(q) \quad , \text{i.e.,} \quad P(r) = \frac{2\pi}{9} G \Sigma_0^2 \left[\frac{\rho(r)}{\rho_0} \right]^{\frac{6}{5}} . \quad (3.16)$$

We plot in fig. 3 the natural logarithm of the normalized distribution function $\mathcal{D}(-\varepsilon)$ eq.(3.11) vs. $-\varepsilon$ for the values $\alpha = 1.4, 1.509$ and 1.6 , appropriate for DM halos. Notice the **linear** behaviour of $\ln \mathcal{D}(-\varepsilon)$ with $-\varepsilon$ which thus indicates an approximately Boltzmann distribution function $\mathcal{D}(-\varepsilon)$. We find that:

- $\mathcal{D}(q)$ and thus $\Psi(q)$ are **positive** for all values of q in the whole range $1 \leq \alpha \leq 2.5$. This shows that the density profiles eq.(3.1) are physically meaningful. Notice that in general there is no guarantee that $\Psi(q)$ from eq.(2.14) will be nowhere negative [11].
- $\ln \mathcal{D}(-\varepsilon)$ is approximately a **linear** function of the energy $-\varepsilon$ for $\alpha \sim 1.5$ in the range of energies $0 < -\varepsilon \lesssim 0.6$ which corresponds to $0 < q \lesssim 7$, that is $0 < r \lesssim 7 r_h$ as can be seen from fig. 3. Therefore, the distribution function $\mathcal{D}(-\varepsilon)$ is approximately a **thermal Boltzman** distribution function in this interval.
- The distribution function $\mathcal{D}(-\varepsilon)$ monotonically decreases for growing energy $-\varepsilon$ as it should be, as can be seen from fig. 3. At fixed ε , $\mathcal{D}(-\varepsilon)$ increases for decreasing α . That is, for decreasing α the density profile is shallower, particles are less gravitationally bounded and particle states with higher energy are populated.

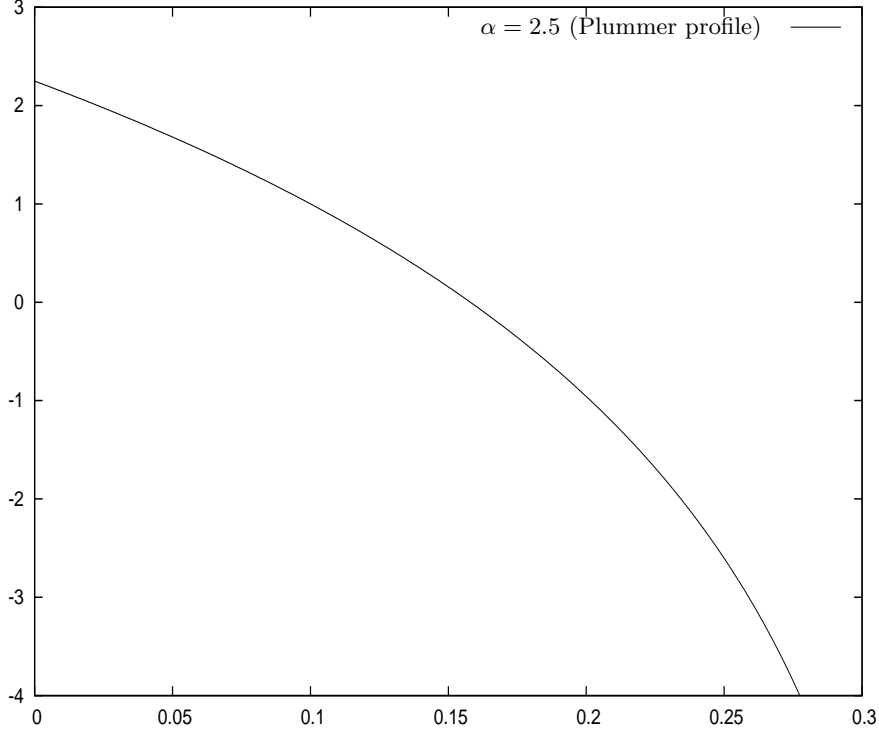


FIG. 4: The natural logarithm of the normalized distribution function $\mathcal{D}(-\varepsilon)$ eq.(3.11) vs. the dimensionless energy $-\varepsilon$ eq.(3.2) for the value $\alpha = 2.5$ which corresponds to the Plummer profile for stellar globular clusters. The distribution function $\mathcal{D}(-\varepsilon)$ is seen to be approximately of Boltzmann type only in the small range $0 \leq -\varepsilon \lesssim 0.07$ corresponding to $0 \leq q < 0.78$.

- The maximum value of $\mathcal{D}(-\varepsilon)$ is at $\varepsilon = 0$. For density profiles appropriate for DM halos ($\alpha \sim 1.5$) we have $\mathcal{D}(0) < 6$ (see fig. 3). For diluted galaxies with $M_h > 10^6 M_\odot$, $r_h > 100$ pc, we find from eqs.(2.14) and (2.16) that the distribution function Ψ is smaller than unity indicating a classical regime. Besides, the Pauli bound for fermionic DM, $\Psi \leq 2$, is fulfilled.
- For comparison we depict in fig. 4 the distribution function for the Plummer (stellar globular cluster) profile ($\alpha = 2.5$). We see that it is approximately thermal only for a small range of energies $0 \leq -\varepsilon \lesssim 0.07$, namely, for $0 \leq q \lesssim 0.78$. Therefore, stars in globular clusters are approximately thermal in a narrower region both in energy and coordinates than the DM in galaxy halos.

Therefore, dark matter described by a cored density profile as eq.(3.1) is **approximately in thermal equilibrium** for $r \lesssim 7 r_h$. It must be recalled that empiric cored density profiles as eq.(3.1) are good approximations to real observational data especially for $\alpha \sim 1.5$.

Notice that the density profiles apply within the virial radius R_{virial} whose typical values are $10 r_h \lesssim R_{virial} \lesssim 100 r_h$ and that the distribution function becomes very small for $q \gtrsim 10$, ($r \gtrsim 10 r_h$).

In the regions where the distribution function $\mathcal{D}(-\varepsilon)$ is approximately Boltzmann-like we can write it as

$$\ln \mathcal{D}(-\varepsilon) = a_0 + b_0 \varepsilon, \quad (3.17)$$

where a_0 is a normalization constant and b_0 eq.(2.7) is related to the temperature T_0 as

$$T_0 = m G \Sigma_0 r_h t_0, \quad t_0 \equiv \frac{4 \pi}{b_0}. \quad (3.18)$$

where

$$G \Sigma_0 r_h = 0.574250 \cdot 10^{-8} \frac{r_h}{\text{kpc}} \frac{\Sigma_0 \text{ pc}^2}{120 M_\odot}. \quad (3.19)$$

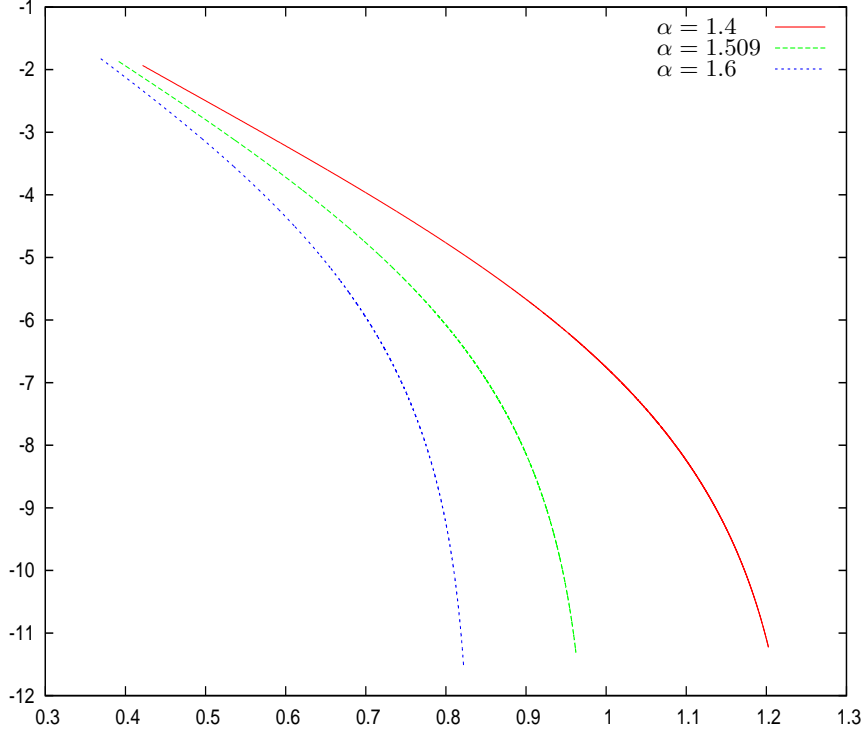


FIG. 5: The natural logarithm of the normalized distribution function $\mathcal{D}(-\varepsilon)$ eq.(3.11) outside the halo radius $r > 3 r_h$ vs. the energy $-\varepsilon$ eq.(3.2) for the DM halo density profiles eq.(3.1) $\alpha = 1.4, 1.509$ and 1.6 . The slope b_0 [eq.(3.17)] of $\mathcal{D}(-\varepsilon)$ vs. $-\varepsilon$ increases for increasing $-\varepsilon$ indicating that the local temperature $t_0 = 4 \pi/b_0$ decreases with r .

From a least square fit to the numerical integration of $\mathcal{D}(-\varepsilon)$ eq. (3.11) for $\alpha = 1.509$, we obtain

$$a_0 = 1.53 \quad , \quad b_0 = 8.72 \quad ,$$

and therefore, we find for the dimensionless temperature t_0 ,

$$t_0 = 1.44 = \mathcal{O}(1) . \quad (3.20)$$

which corresponds to

$$\frac{T_0}{m} \sim 10^{-8} \frac{r_h}{\text{kpc}} \frac{\Sigma_0 \text{ pc}^2}{120 M_\odot} . \quad (3.21)$$

More precisely,

$$T_0 = 0.1333 t_0 \frac{m}{2 \text{ keV}} \frac{r_h}{\text{kpc}} \frac{\Sigma_0 \text{ pc}^2}{120 M_\odot} \text{ K} = 0.192 \frac{m}{2 \text{ keV}} \frac{r_h}{\text{kpc}} \frac{\Sigma_0 \text{ pc}^2}{120 M_\odot} \text{ K} . \quad (3.22)$$

For m in the keV scale (warm dark matter), T_0 runs from the mili-Kelvin for dwarf galaxies till tens of Kelvin for the largest galaxies [16].

We plot in fig. 5 the natural logarithm of the distribution function $\mathcal{D}(-\varepsilon)$ eq.(3.11) outside the halo radius $r > 3 r_h$ for $\alpha = 1.4, 1.509$ and 1.6 vs. the energy $-\varepsilon$. We see that the slope of $\mathcal{D}(-\varepsilon)$ vs. $-\varepsilon$ increases for increasing $-\varepsilon$. From eqs.(3.17) and (3.18), an increasing slope implies an increasing b_0 and therefore the dimensionless temperature $t_0 = 4 \pi/b_0$ is not constant outside $r = 3 r_h$ as it is inside $r = r_h$. This suggests that $t_0 = 4 \pi/b_0$, and therefore T_0 , can be considered a **local temperature** that slowly decreases with r for $r > 3 r_h$.

As shown in sec. V below, this local character of the temperature is supported by the computation of the velocity dispersion.

D. The Pauli bound on the distribution function

Expressing the halo radius r_h in terms of the halo mass M_h in eq.(2.16) with the help of the scaling relation eq.(3.7) yields for the distribution function

$$\Psi(q) = 0.00531939 \left(\frac{10^6 M_\odot}{M_h} \right)^{\frac{5}{4}} \left(\frac{\Sigma_0 \text{ pc}^2}{120 M_\odot} \right)^{\frac{3}{4}} \left(\frac{2 \text{ keV}}{m} \right)^4 \mathcal{D}(q) . \quad (3.23)$$

The Pauli bound for spin-1/2 DM particles requests that $\Psi(q) \leq 2$. The distribution function takes its maximum value at the halo center $q = 0$ where $\mathcal{D}(0) = 4.914245$ for $\alpha = 1.509$. Thus, from eq.(3.23), the Pauli bound is everywhere satisfied provided the halo mass is bounded from below as

$$M_h \geq 3.11 \cdot 10^4 M_\odot \left(\frac{\Sigma_0 \text{ pc}^2}{120 M_\odot} \right)^{\frac{3}{5}} \left(\frac{2 \text{ keV}}{m} \right)^{\frac{16}{5}} .$$

This lower bound corresponds to the degenerate limit of quantum fermions [16] showing the consistency of the distribution function obtained from the Eddington equation with the quantum treatment of the DM in ref. [5, 7, 15, 16].

IV. THE HALO DARK MATTER EQUATION OF STATE

We compute now the DM equation of state from the pressure eq.(3.12)-(3.13) and the density profile eq.(3.1). We obtain from eqs.(2.22) and (3.12)

$$\frac{P(r)}{\rho(r)} = \frac{1}{3} v^2(r) = G \Sigma_0 r_h \frac{\Pi(q)}{F(q)} . \quad (4.1)$$

We plot in fig. 6 the normalized ratio $P(r)/\rho(r)$:

$$\frac{1}{G \Sigma_0 r_h} \frac{P(r)}{\rho(r)} ,$$

versus the distance q for several values of α .

We see that for $\alpha \sim 1.5$ inside the halo radius $r < r_h$ ($q < 1$) the normalized ratio $P(r)/\rho(r)$ and thus the velocity dispersion $v^2(r)/3$ turn to be **approximately constant** (independent of r). This implies that the dark matter obeys locally, at each point, an ideal gas equation of state

$$P(r) = \frac{T(r)}{m} \rho(r) \quad , \quad T(r) \equiv m G \Sigma_0 r_h t(q) \quad , \quad t(q) \equiv \frac{\Pi(q)}{F(q)} . \quad (4.2)$$

The local temperature $T(r)$ is related to the dispersion velocity by the usual relation

$$T(r) = \frac{1}{3} m v^2(r) . \quad (4.3)$$

The temperature $T(r)$ is **approximately constant** $\simeq T_0$ inside the halo radius for $\alpha \sim 1.5$ as shown by figs. 6 and 8. More precisely, for $\alpha = 1.509$, $T(q)$ is the closest to a constant inside the halo $0 < q < 1$:

$$t(q) \simeq 1.419 \quad , \quad 0 < q < 1 \quad , \quad \alpha = 1.509 . \quad (4.4)$$

Namely, for $\alpha = 1.509$ dark matter in the galaxy halo is closest to thermal equilibrium for the density profile eq.(3.1).

We see that inside the halo, the value of the dimensionless temperature $t(q)$ eq.(4.4) obtained here from the equation of state, as well as from the distribution function in eq.(3.20) are approximately equal.

We see from eq.(3.22) that the galaxy temperature T_0 grows **linearly** with the halo radius. T_0 can be expressed in terms of the halo mass using eq.(3.7) with the coefficient d_α corresponding to the case closest to thermal equilibrium, $\alpha = 1.509$, $d_{1.509} = 2.18188$, with the result:

$$r_h = 61.801 \sqrt{\frac{M_h}{10^6 M_\odot} \frac{120 M_\odot}{\Sigma_0 \text{ pc}^2}} \text{ pc} \quad , \quad T_0 = 8.238 t(q) \frac{m}{2 \text{ keV}} \sqrt{\frac{\Sigma_0 \text{ pc}^2}{120 M_\odot} \frac{M_h}{10^6 M_\odot}} \text{ mK} .$$

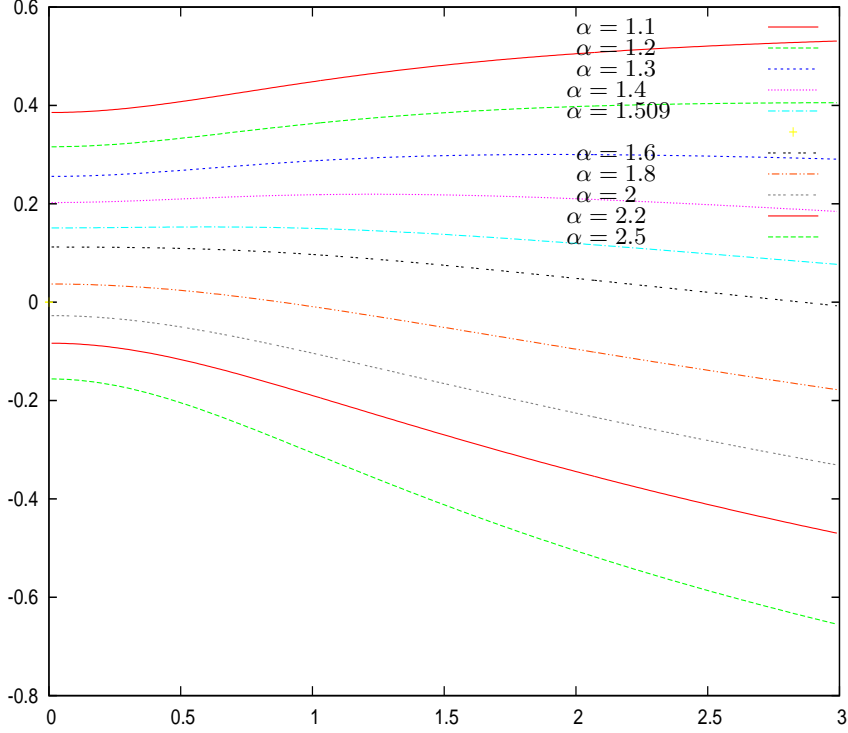


FIG. 6: The ordinary logarithm of the normalized ratio $\frac{1}{G \Sigma_0 r_h} \frac{P(r)}{\rho(r)} = T(q)/[m G \Sigma_0 r_h] = \Pi(q)/F(q) = t(q)$ (or dimensionless temperature) vs. q for several values of the exponent α , $1 < \alpha \leq 2.5$ in the density profile eq.(3.1). The best fitting values for DM halos are in the range $1.2 < \alpha < 1.5$. We see that the temperature is **approximately constant** inside the halo radius $q < 1$ for $\alpha \sim 1.5$.

Hence, the galaxy temperature T_0 grows as the square root of the halo mass.

For $q \gtrsim 1$, the local temperature decreases. In fig. 8 we plot $t(q)$ vs. $\log_{10} q$ for $\alpha = 1.509$. We see from fig. 8 that the local temperature $t(q)$ decreases slowly with q . For instance, $t(q = 10) \simeq \frac{1}{2} t(q < 1)$ and $t(q = 100) \simeq 0.095 t(q < 1)$. In other words, the DM is not in global thermal equilibrium for $q > 1$ but there is a **local** thermal equilibrium with a local normalized temperature $t(q)$ that decreases slowly when one gets farther from the center.

A local temperature for $q \gtrsim 1$ follows by fitting the distribution function $\mathcal{D}(q)$ to a Boltzmann-like form for $q \gtrsim 1$ as in eq.(3.17): a local decreasing temperature t_0 with a similar behaviour to eq.(4.2) is obtained, showing that the concept of a local q -dependent temperature, slowly varying with the coordinates is perfectly consistent in the region $r \gtrsim r_h$ of the DM galaxy halo.

A. Polytrropic behaviour of the equation of state

We plot in fig. 7 the ordinary logarithm of the normalized pressure

$$\Pi(q) = \frac{P(r)}{G \Sigma_0^2},$$

as a function of the ordinary logarithm of the normalized density

$$F(q) = \frac{\rho(r)}{\rho_0},$$

where we used eqs.(2.6) and (3.12).

We see from fig. 7 that the pressure behaves in good approximation as a power of the density:

$$P = A \rho^\gamma \quad , \quad \Pi = a F^\gamma \quad , \quad A = G r_h^2 \rho_0^{2-\gamma} a \quad , \quad (4.5)$$

α	γ	a
1.509	1.05	1.46
2.5	1.2	0.698

TABLE I: The polytropic index γ and the amplitude a in the polytropic equation of state for the DM cored profile $\alpha = 1.509$ and for stellar globular clusters described by the Plummer profile.

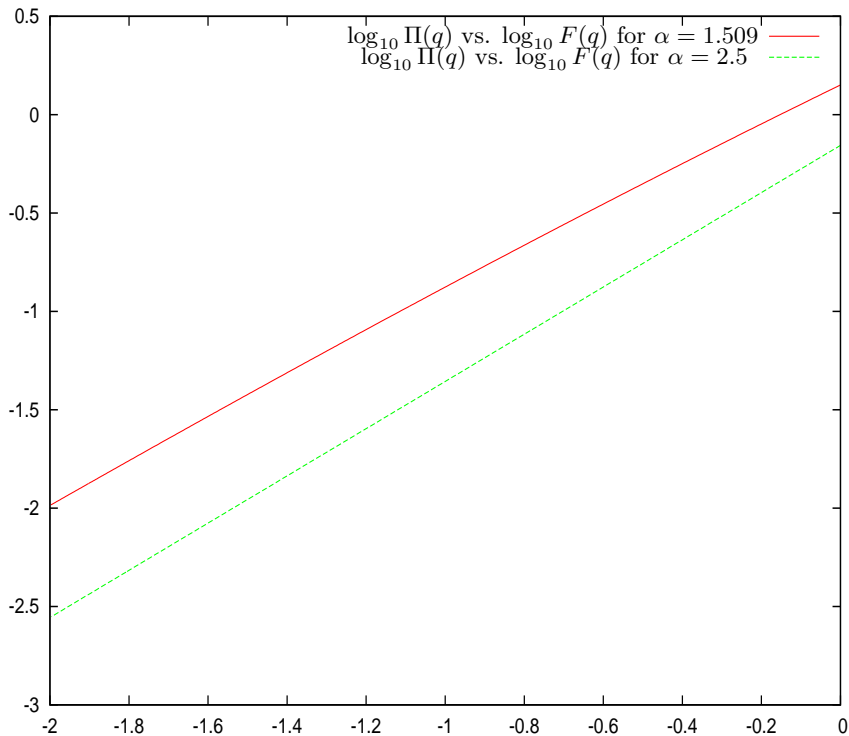


FIG. 7: The ordinary logarithm of the normalized pressure $\Pi(q)$ eq.(3.12) vs. the ordinary logarithm of the normalized density $F(q)$ eq.(2.6) for the dark matter cored profile $\alpha = 1.509$ and for the Plummer (stellar globular cluster) profile ($\alpha = 2.5$). The straight lines obtained in this log-log plot correspond to the polytropic equations of state in eq.(4.5).

where A , a and γ are constants.

We display in Table I the values of γ and a for the DM halo profile $\alpha = 1.509$ and for the Plummer (stellar globular cluster) profile $\alpha = 2.5$. γ and a are obtained by a least-square fit to the numerical values of $\Pi(q)$ and $F(q)$ for $\alpha = 1.509$ in the relevant region $0 < r < R_{virial}$ and from eq.(3.16) in the Plummer case. The obtained polytropic indexes are

$$\gamma_{halo} = 1.05 \quad \text{and} \quad \gamma_{Plummer} = 1.2.$$

In the Plummer case of stellar globular clusters ($\alpha = 2.5$) the polytropic index $\gamma = 1.2$ is an exact result valid for all density values eq.(3.16).

V. GALAXY HALOS TURN TO BE IN APPROXIMATE LOCAL THERMAL EQUILIBRIUM

Once the galaxy is formed, it is in a virialized stationary state of size $R_{virial} : 0 \leq r \leq R_{virial}$.

The virialized region is in an approximate **local** thermal equilibrium situation, namely at each point r , the equation of state is that of an ideal self-gravitating gas with a local velocity dispersion $v^2(r) = 3 T(r)/m$ which slowly varies with r . The local temperature $T(r)$ slowly varies with r too.

Inside the halo radius $r \lesssim r_h$, $v^2(r)$ and $T(r)$ are approximately constant as shown in fig. 6. This region is in **approximate thermal equilibrium**.

It is instructive to look to the analytic expression of $t(q)$ for $\alpha = \frac{3}{2}$ that follows from eqs.(3.15) and (4.2):

$$t(q) = 4 \pi \left[\frac{1}{2} \sqrt{1+q^2} + (1+2q^2)(1+q^2) \frac{\text{Arg Sinh}(q)}{q} - (1+q^2)^{\frac{3}{2}} \ln[4(1+q^2)] \right] , \quad \alpha = \frac{3}{2} , \quad (5.1)$$

Expanding this function in powers of q^2 yields

$$\begin{aligned} t(q) &= 8 \pi \left[\frac{3}{4} - \ln 2 + \frac{3}{2} \left(\frac{25}{36} - \ln 2 \right) q^2 - \frac{3}{8} \left(\ln 2 - \frac{41}{60} \right) q^4 + \frac{1}{16} \left(\ln 2 - \frac{269}{420} \right) q^6 + \mathcal{O}(q^8) \right] = \\ &= 1.428867 [1 + 0.0342269 q^2 - 0.0647319 q^4 + 0.0579028 q^6 + \mathcal{O}(q^8)] \end{aligned} \quad (5.2)$$

We see that this series which converges for $|q| < 1$, has small and alternating sign coefficients. This is an explanation why $t(q)$ is practically constant for $\alpha \simeq \frac{3}{2}$ and $q \lesssim 1.5$ as shown in fig. 6.

Beyond the halo radius, in the region $r_h \lesssim r \leq R_{virial}$, $v^2(r)$ and $T(r)$ slowly decrease with r as shown in fig. 8.

It is illuminating to consider here the circular velocity

$$v_c^2(r) \equiv \frac{G M(r)}{r} , \quad (5.3)$$

and in analogy with eq.(4.3), we associate to $v_c^2(r)$ the circular temperature

$$T_c(r) \equiv \frac{1}{3} m v_c^2(r) . \quad (5.4)$$

From eqs.(3.5) and (4.2) we have respectively,

$$\begin{aligned} v_c^2(r) &= 4 \pi G \rho_0 r_h^2 \frac{w_\alpha(q)}{q} , \\ T_c(r) &= m G \rho_0 r_h^2 t_c(q) , \quad t_c(q) \equiv \frac{4 \pi}{3} \frac{w_\alpha(q)}{q} . \end{aligned} \quad (5.5)$$

We plot in fig. 8 the normalized temperature $t(q)$ and the circular temperature $t_c(q)$ vs. $\log_{10} q$ for $\alpha = 1.509$. We clearly see approximate thermal equilibrium inside the halo radius $r < r_h$, ($q < 1$).

Outside the halo $r \gtrsim r_h$, ($q \gtrsim 1$) the local temperatures $t(q)$ and $t_c(q)$ decrease slowly with the distance to the center r . Moreover, we see in fig. 8 that the local temperature $t(q)$ **follows** the decrease of the circular temperature $t_c(q)$ in this region $q \gtrsim 1$. Around $q = 10$ we find $t(q) \simeq 0.8 t_c(q)$

More precisely, we can compare the large distance asymptotic behaviour of the local temperature $t(q)$ for $\alpha = 3/2$ given by eq.(5.1) with that of the circular temperature $t_c(q)$ that follows from eqs.(3.4) and (5.5):

$$\begin{aligned} t(q) &\stackrel{q \gg 1}{\simeq} \frac{\pi}{q} \left[\ln(2q) - \frac{3}{4} \right] \left[1 + \mathcal{O}\left(\frac{1}{q^2}\right) \right] , \\ t_c(q) &\stackrel{q \gg 1}{\simeq} \frac{4\pi}{3q} [\ln(2q) - 1] \left[1 + \mathcal{O}\left(\frac{1}{q^2}\right) \right] , \end{aligned} \quad (5.6)$$

We see from eq.(5.6) that the temperature $t(q)$ and the circular temperature $t_c(q)$ exhibit the same analytic structure for $q \gtrsim 5$. Asymptotically, $t_c(q)$ is larger than $t(q)$ by a factor $4/3$:

$$\frac{t_c(q)}{t(q)} \stackrel{q \gg 1}{\simeq} \frac{4}{3} \left[1 - \frac{1}{4 \ln(2q) - 3} + \mathcal{O}\left(\frac{1}{q^2}\right) \right] , \quad (5.7)$$

As shown by fig. 8, $t_c(q)$ is larger than $t(q)$ by a factor going approximately from unity at $q = 2.93$ to 1.3 at $q = 160$ and reaching the limiting value $4/3$ at $q = \infty$ as follows from eq.(5.7).

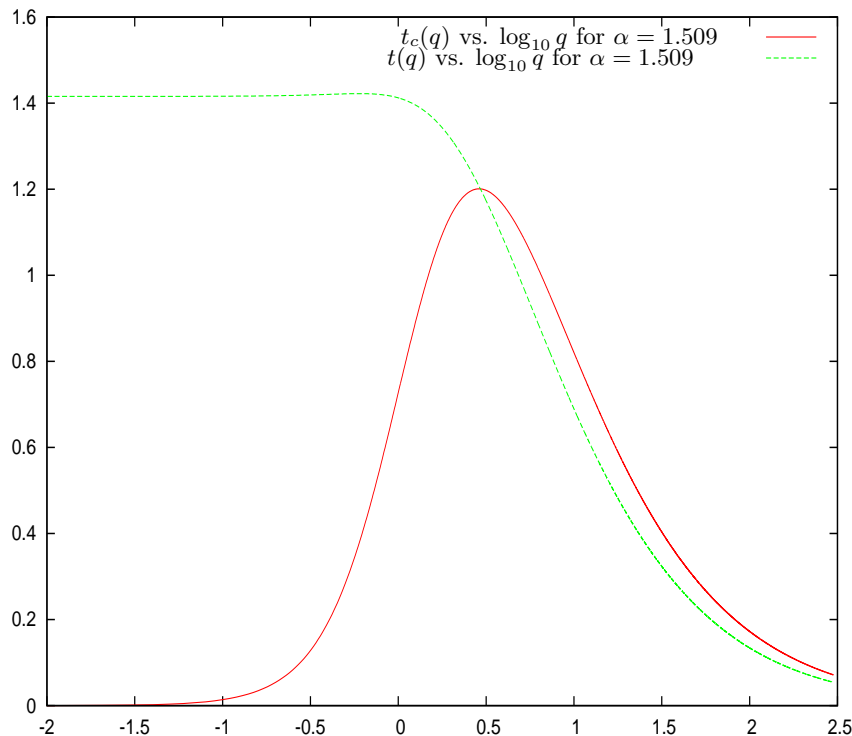


FIG. 8: The normalized temperature $t(q)$ and the circular temperature $t_c(q)$ vs. $\log_{10} q$ for $\alpha = 1.509$. It clearly displays approximate thermal equilibrium inside the halo radius $q < 1$. For $q \gtrsim 1$ it shows local thermal equilibrium with a normalized temperature $t(q)$ that decreases slowly with q following the decreasing circular temperature $t_c(q)$.

Moreover, it must be noticed that the local temperature $T(r)$ obtained from the local velocity dispersion eq.(4.3) agrees with the local temperature obtained from the distribution function $\mathcal{D}(-\varepsilon)$ eq.(3.11) outside the halo radius $r > 3 r_h$ through eqs.(3.17)-(3.18) discussed at the end of sec. III C. This agreement shows the consistency of the concept of a local halo decreasing temperature for $r \gtrsim r_h$.

Physically, these phenomena are clearly understood because in the inner halo region $r \lesssim r_h$, the density is higher than in the region beyond the halo radius. The gravitational interaction in the inner region is strong enough and thermalizes the self-gravitating gas of DM particles while beyond the halo radius the particles are too dilute to reach thermalization, namely, although they are virialized, they had not time to thermalize. Notice that virialization always starts before than thermalization [18].

In the process of thermalization there is a transfer flow of potential energy into kinetic energy [18]. Clearly, in the region $r \gtrsim 3 r_h$ which is only thermalized at local level we find that the kinetic energy is lower, and therefore the local temperature is lower than the temperature in the internal region $r < r_h$ where thermalization is already achieved.

This treatment applies to dilute large galaxies which are in a classical physics regime for halo masses $M_h > 10^6 M_\odot$.

For smaller (dwarf) galaxies there is not yet available information on density profiles from observations in order to determine $F(q)$. Knowing $F(q)$ for dwarf galaxies will allow to apply the methods developed here to find the phase-space distribution function $f(E)$ and the velocity dispersion $v^2(r)$ for dwarf galaxies.

Notice that the Thomas-Fermi approach to galaxy structure applies to **all types of galaxies** and allows to determine theoretically all physical magnitudes for them [6]-[7]. In the classical regime, for halo masses $M_h > 10^6 M_\odot$, the galaxy equation of state computed in the Thomas-Fermi approach yields the same results as found here from the empirical α -profiles and the Eddington equation, namely the Boltzmann self-gravitating ideal gas equation of state, which shows the robustness of these results.

This paper provides an unified framework in which galaxy structure is obtained from the DM gas of particles in analogous way as globular clusters structure is obtained from a gas of stars.

For dwarf galaxies, the equation of state derived in the Thomas-Fermi theory exhibits deviations from the Boltzmann ideal gas equation of state due to macroscopic quantum effects well accounted by the Thomas-Fermi approach [6]-[7] and which reflect the quantum fermion state near degeneration characteristic of dwarf compact galaxies.

Acknowledgments

We thank Paolo Salucci for useful discussions.

VI. APPENDIX

We compute in this Appendix the integral eq.(2.19).

We insert the integral representaion for $\Psi(-\nu')$ given by eq.(2.11)

$$J(\nu) \equiv \int_{\nu(\infty)}^{\nu} d\nu' (\nu - \nu')^{\frac{3}{2}} \Psi(-\nu') = \sqrt{2} \pi \frac{\rho_0}{m^{\frac{5}{2}} T_0^{\frac{3}{2}}} \int_{\nu(\infty)}^{\nu} d\nu' (\nu - \nu')^{\frac{3}{2}} \int_{\nu(\infty)}^{\nu'} \frac{d\nu''}{\sqrt{\nu' - \nu''}} \frac{d^2 F}{d\nu''^2}.$$

Interchanging the integration over ν' and ν'' yields

$$J(\nu) = \sqrt{2} \pi \frac{\rho_0}{m^{\frac{5}{2}} T_0^{\frac{3}{2}}} \int_{\nu(\infty)}^{\nu} d\nu'' \frac{d^2 F}{d\nu''^2} \int_{\nu''}^{\nu} \frac{(\nu - \nu')^{\frac{3}{2}}}{\sqrt{\nu' - \nu''}} d\nu'.$$

The integral over ν' can be performed explicitly with the result

$$\int_{\nu''}^{\nu} d\nu' \frac{(\nu - \nu')^{\frac{3}{2}}}{\sqrt{\nu' - \nu''}} = \frac{3}{8} \pi (\nu - \nu'')^2,$$

and therefore,

$$J(\nu) = \frac{3\pi^2}{4\sqrt{2}} \frac{\rho_0}{m^{\frac{5}{2}} T_0^{\frac{3}{2}}} \int_{\nu(\infty)}^{\nu} d\nu'' (\nu - \nu'')^2 \frac{d^2 F}{d\nu''^2}.$$

as in eq.(2.19).

-
- [1] R. F. G. Wyse, G. Gilmore, IAU Symposium, Vol. 244, p. 44-52 (2007), arXiv:0708.1492. J. van Eymeren et al. A & A 505, 1-20 (2009). W. J. G. de Blok, Advances in Astronomy, vol. 2010, pp. 1-15, (2010), arXiv:0910.3538. P. Salucci, Ch. Frigerio Martins, arXiv:0902.1703, EAS Publications Series, 36, 2009, 133-140.
- [2] G. Gilmore et al., Ap J, 663, 948 (2007).
- [3] M. Walker, J. Peñarrubia, Ap. J. 742, 20 (2011).
- [4] D. Boyanovsky, H. J. de Vega, N. G. Sanchez, arXiv:0710.5180, Phys. Rev. **D 77**, 043518 (2008).
- [5] H. J. de Vega, P. Salucci, N. G. Sanchez, New Astronomy **17**, 653 (2012).
- [6] C. Destri, H. J. de Vega, N. G. Sanchez, New Astronomy **22**, 39 (2013).
- [7] C. Destri, H. J. de Vega, N. G. Sanchez, Astrop. Phys., **46**, 14 (2013).
- [8] I. M. Gelfand, G. E. Shilov, 'Generalized Functions', Academic Press, New York, 1964.
- [9] A. S. Eddington, MNRAS 76, 572 (1916).
- [10] H. C. K. Plummer, MNRAS 71, 460 (1911) and 76, 107 (1915).
- [11] J Binney, S. Tremaine, 'Galactic Dynamics', Princeton Univ. Press, 2008.
- [12] T. Padmanabhan, 'Structure Formation in the Universe', Cambridge Univ. Press, 1995.
- [13] A. P. Prudnikov, Yu. A. Brichkov, O. I. Marichev, 'Integrals and Series' vol. 3, Nauka, Moscow, 1986.
- [14] Paolo Salucci, private communication.
- [15] H. J. de Vega, P. Salucci, N. G. Sanchez, arXiv:1309.2290.
- [16] H. J. de Vega, N. G. Sanchez, arXiv:1310.6355.
- [17] I. S. Gradshteyn, I. M. Ryzhik, Table of Integrals, Series, and Products, Academic Press, San Diego, 1994.
- [18] C. Destri, H. J. de Vega, Phys. Rev. **D 73**, 025014 (2006).
- [19] H. J. de Vega, P. Salucci, N. G. Sanchez, New Astronomy **17**, 653 (2012).
- [20] F. Donato et al., MNRAS **397**, 1169 (2009).
- [21] J Kormendy, K C Freeman, IAU Symposium, Sydney, 220, 377 (2004), arXiv:astro-ph/0407321.
- [22] M. Spano et al., MNRAS, 383, 297 (2008).